Time domain terahertz impulse ranging studies

R. A. Cheville and D. Grischkowsky
School of Electrical and Computer Engineering and Center for Laser Research, Oklahoma State University, Stillwater, Oklahoma 74078

(Received 28 June 1995; accepted for publication 25 July 1995)

We present time domain impulse scattering measurements of freely propagating terahertz radiation measured with subpicosecond resolution. This fast time response corresponds to a usable bandwidth of over 1 THz. Measured scattered fields from thin wire targets agree well with the calculated scattering for the early and late time response in both the time and frequency domains. Realistic ranging from scale model aircraft is demonstrated. © *1995 American Institute of Physics.*

Freely propagating electromagnetic energy has been used extensively to detect and identify objects at a distance. Since the field scattered from all but the simplest of objects cannot be exactly calculated, a wide variety of techniques have been proposed to identify objects by the radiation scattered from them.[1] It has been recognized since the 1950s that the late time response to an impulse signal provides an intuitive and potentially simple way to identify targets.[2,3] Impulse techniques have several experimental advantages over single frequency methods for scale ranging including the elimination of interfering background signals and simultaneous acquisition of many frequencies. Such advantages have led to several recent studies using both electronic[4,5] and optoelectronic[6–9] methods to observe the response of simple geometrical targets. All electronic methods have achieved a bandwidth of 20 GHz (Ref. 5) while the fastest optoelectronic results reported to date have a bandwidth of 140 GHz.[6]

In this letter we use optoelectronic techniques to generate single cycle pulses of freely propagating radiation with frequency components extending beyond 1 THz, and demonstrate ultrawide bandwidth scattering from simple geometrical objects. These pulses are the best approximation to impulse excitation ever used in ranging studies. The absolute bandwidth is also larger than any other previously reported. The relatively short wavelengths of the THz pulse permit target features of less 1 mm to be observed, making this technique ideal for scale ranging measurements since realistic target to wavelength ratios can be maintained. Furthermore, the measurement window achieved by the optoelectronic gating technique enables only the scattered signal from the target to be detected, providing background free measurements.

The optoelectronic technique used is similar to that previously employed for THz time domain spectroscopy.[10] The experimental setup is shown in Fig. 1(a). To measure scattering from objects, the system alignment is first optimized with the flat deflecting mirrors removed from the THz beam [dashed position in Fig. 1(a)]. The deflecting mirrors are then inserted to direct the THz beam towards the target. The distances in Fig. 1(a) are roughly to scale, but the target size has been increased 20× for clarity. The focal length f of the paraboloidal mirrors is 11.9 cm, the deflecting mirrors are 20 cm from the center of the paraboloidal mirrors, and the target is 64 cm from the deflecting mirrors. A helium neon laser aligned coincident with the THz beam permits accurate positioning of the targets. All THz components and associated optics are on a breadboard 30 cm above the optical table to avoid spurious reflections. Targets can be positioned up to 190 cm from the deflecting mirrors, limited by the size of the airtight enclosure purged with dry air to mitigate absorption by water vapor.

The THz beam has a Gaussian profile with a waist at the face of the silicon lens.[11] The off-axis paraboloidal mirror, located a focal distance $f=11.9$ cm from the surface of the silicon lens, generates a second waist, whose diameter is proportional to wavelength, a distance f beyond the mirror, as shown in Fig. 1(a). At large distances beyond this second waist, the divergence angle (FWHM) of the propagating THz beam approaches 35 mrad, independent of wavelength. For the 64 cm target distance the beam radius ($1/e$ points in field) at 1 THz (0.3 mm wavelength) was 1.6 cm at the target. To a good approximation frequencies above 0.5 THz have a uniform distribution over the beam profile at the target. This well-characterized THz beam with a source to target distance of more than 1000 wavelengths at 0.5 THz offers significant advantages for ranging studies.

To measure the incident pulse a large flat aluminum mirror was used in place of the target, permitting the response of the receiver to be separated from the scattered field.[7] A typical pulse reflected from the mirror is shown in Fig. 1(b) and the corresponding amplitude spectrum, obtained by the numerical Fourier transform of the time data, is shown in Fig. 1(c). The pulse has a double Gaussian shape with the positive part of the pulse having a FWHM of 0.6 ps. The extended structure following the pulse is due to residual water vapor in the enclosure. As shown in Fig. 1(c), the measurable frequency components of the incident pulse extended from 100 GHz to ~2 THz. The water vapor absorption is clearly visible as sharp absorption lines in the spectrum.

To compare with the earlier, lower frequency work,[6] we demonstrate THz impulse ranging with conducting cylinders (wires) as targets. For a plane wave incident upon a conducting cylinder, the scattered field may be calculated exactly.[12] Unlike a sphere, the response of the cylinder is dependent upon the orientation of the cylinder to the polarization of the incident electric field, permitting different responses to be achieved simply by rotating the target. Signal strengths are larger for a cylinder since the scattered field has an inverse square root dependence on the distance from the target, as opposed to inverse distance dependence for a sphere. The

 0003-6951/95/67(14)/1960/3/$6.00

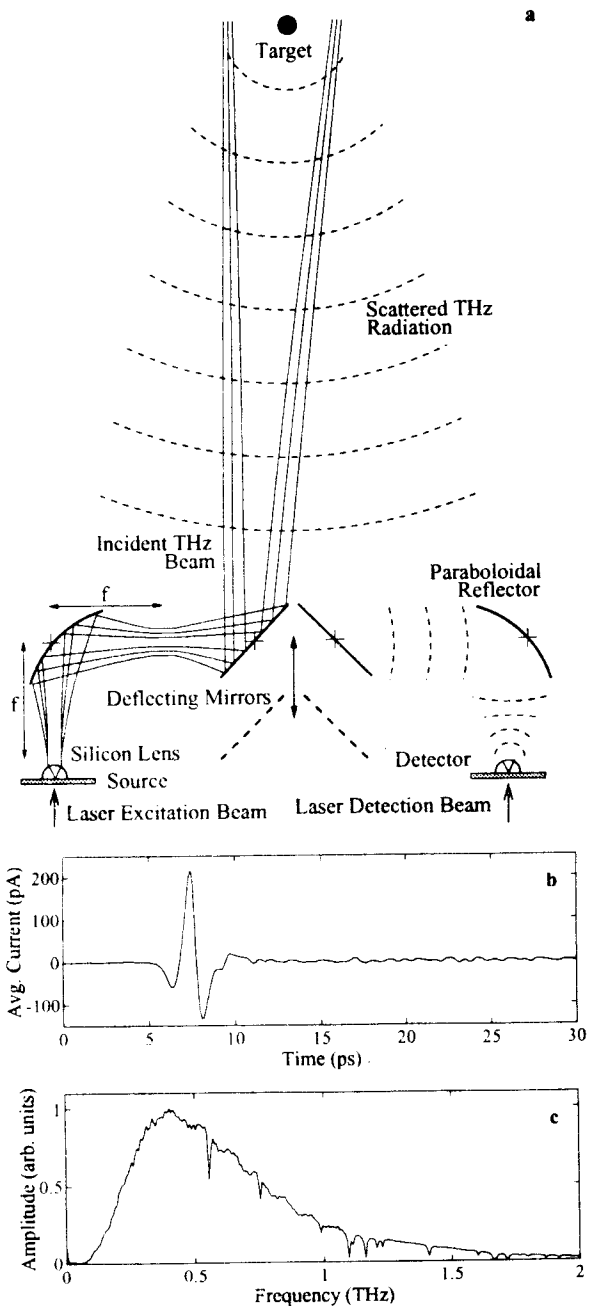

FIG. 1. (a) Experimental setup used for THz ranging studies. (b) Pulse incident on target, measured using a flat mirror. (c) Amplitude spectrum of pulse in (b) showing frequency components to 2 THz.

results presented here were obtained from bare copper wires of 0.26, 0.51, and 1.02 mm diameter. The wire extended well beyond the extent of the THz beam. The angle between the incident and measured scattered wave was less than 7°. The wire targets were located 64 cm from the centers of the deflecting mirrors.

Figure 2 shows the scattered pulse from a 0.51 diam wire oriented both (a) perpendicular and (b) parallel to the incident electric field. For the wire oriented perpendicular to the incident field, the electric field of the THz radiation induces a pulse of current on the wire which propagates as a creeping wave around the circumference of the wire.[13] After

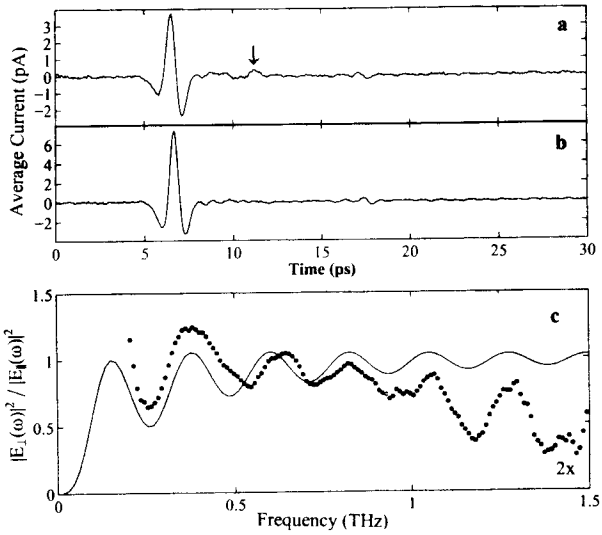

FIG. 2. Scattered field from 0.51 mm diam wire oriented (a) perpendicular and (b) parallel to the incident electric field. The data shown are an average of 12 scans. The measured ratio $|E_{sc,\perp}(\omega)|^2/|E_{sc,\parallel}(\omega)|^2$ (dots) is plotted in (c) along with the calculated ratio (solid line).

traveling fully around the wire the reradiated pulse propagates back towards the detector. This reradiated pulse is identified by an arrow in Fig. 2(a). For a wire parallel to the incident electric field the generated current pulse travels along the wire, and is not seen by the detector [Fig. 2(b)]. This intuitive picture illustrates why time domain scattering measurements can often be more understandable than those in the frequency domain.

The scattered field in the frequency domain for a plane wave incident upon an infinite perfectly conducting cylinder may be calculated exactly for both wire orientations and is given by[12–14]

$$E_{sc}(\omega)=E_{inc}(\omega)\sqrt{\frac{2}{\pi k_0 r}}\,e^{i(k_0 r-\pi/4)}T(\phi), \tag{1}$$

where $E_{sc}(\omega)$ is the scattered field, $E_{inc}(\omega)$ is the incident field, r is the distance from the scatterer to the detector, $k_0=2\pi/\lambda$ is the wave vector, and $T(\phi)$ depends upon the target composition, polarization of the incident wave relative to the wire orientation, and the angle ϕ between the incident and scattered wave. For a perfect conductor and backscattering (ϕ=0) the T terms for incident field both parallel and perpendicular to the wire are[14]:

$$T_\parallel=\sum_{n=0}^{\infty}\epsilon_n(-1)^n\frac{-J_n(k_0a)}{H_n^{(1)}(k_0a)}, \tag{2}$$

$$T_\perp=\sum_{n=0}^{\infty}\epsilon_n(-1)^n\frac{-J_n'(k_0a)}{H_n^{(1)\prime}(k_0a)}, \tag{3}$$

$J_n, H_n^{(1)}$ are Bessel and Hankel functions respectively, with the prime denoting the derivative with respect to k_0a. ϵ_n is 1 for $n=0$ and 2 otherwise, and the wire radius is a. The frequency and angle dependent scattering is often expressed as a cross section, $\sigma(\omega)=4|T|^2/k_0\sim|E_{sc}(\omega)|^2$ for fixed distance.

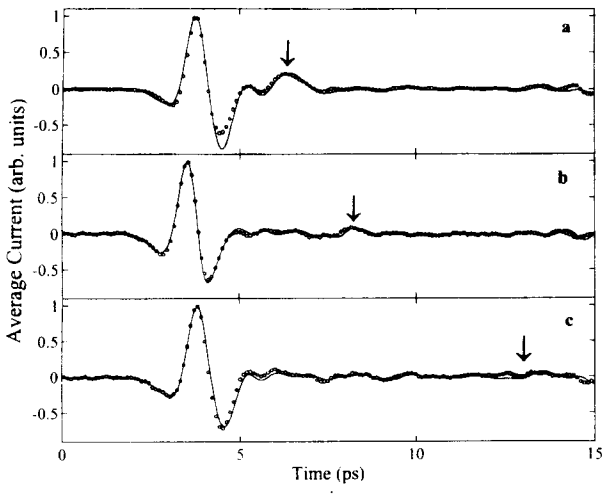

FIG. 3. Response of (a) 0.26, (b) 0.51, and (c) 1.02 mm diam wires oriented perpendicular to the incident field. Measured (dots) and calculated (solid line) results.

The scattering cross-section ratio of $\sigma_\perp/\sigma_\parallel$ calculated by a numerical summation to $n=100$ is plotted as a solid line in Fig. 2(c). The measured scattered field, $E_{sc}(\omega)$, is calculated by applying a numerical Fourier transform to the time domain data in Figs. 2(a) and 2(b). The ratio $|E_{sc\perp}(\omega)|^2/|E_{sc\parallel}(\omega)|^2$ is equal to $\sigma_\perp/\sigma_\parallel$ and is plotted as points in the figure, normalized by a factor of 2. Oscillatory structure is clearly visible out to 1.5 THz, with agreement between the measured and calculated values to around 1 THz. The error in amplitude is possibly due to angular misalignment of the wire axis perpendicular to the plane of the incident THz beam, or to the assumption of a perfectly polarized field. The most significant source of error is the phase difference of the incident beam over the extent of the target due to the finite radius of curvature of the THz phase front. This is especially severe for the higher frequencies where the phase of the incident beam varies more rapidly over the target. The phase difference at 1 THz between the center of the beam (radius of curvature=78.6 cm) and the $1/e$ point (field) is approximately π radians at the target.

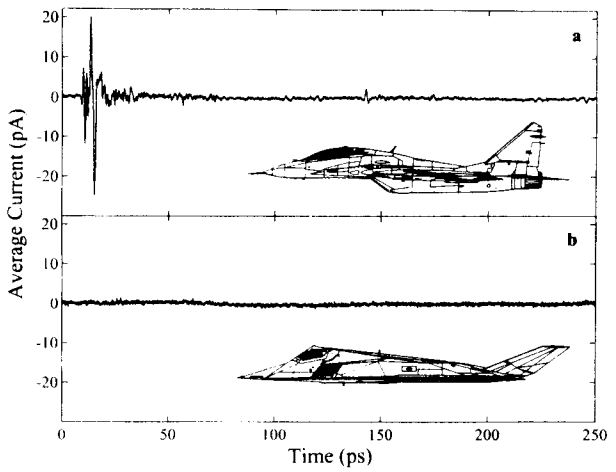

FIG. 4. (a) Scattered field from 1/200th scale MiG-29 aircraft model in profile (see Ref. 15). (b) Scattered field from model F-117A "Stealth" fighter aircraft in profile (see Ref. 15).

Given the incident pulse shape, the exact response of the wire may also be calculated in the time domain. The scattered field in the time domain $E_{sc}(t)$, is calculated by inverse Fourier transform of Eq. (1). Figure 3 shows the measured and calculated pulse shapes in the time domain for three wire diameters. All wires in this case are oriented perpendicular to the incident electric field. There is good agreement between the calculated and measured response (normalized to fit) in all cases. The reradiated pulse due to the creeping wave (indicated by arrows in Fig. 3) is delayed in time proportional to the wire diameter. The other oscillations are due to residual water vapor in the enclosure.

To observe the response of realistic targets with a more complex late time response, we used metal model aircraft with target/wavelength ratios of practical interest. Two 1/200th scale model aircraft, an MiG-29 Fulcrum and F-117A Stealth,[15] were located 107 cm from the deflecting mirrors and oriented in profile as shown in Fig. 4. The target to wavelength ratio for the 1/200th scale model and the 100 GHz–2 THz frequency range correspond to measuring the scattered field from 0.5 to 10 GHz of a full size target at 230 m distance. The time domain response for the MiG-29 has an extensive signal after the initial specular reflection. The lack of a scattered signal for the Stealth aircraft within our signal-to-noise ratio indicates the effectiveness of the aircraft's geometry, designed to reflect energy away from the detector.

This work was partially supported by the National Science Foundation.

[1] Y. H. Mao, in *Advanced Radar Techniques and Systems*, edited by G. Galati (Peregrinus, London, 1993).
[2] E. M. Kennaugh and R. L. Cosgriff, National Convention IRE Record, Pt. I, 1958.
[3] E. M. Kennaugh and D. L. Moffatt, Proc. IEEE **53**, 893 (1965).
[4] H. C. Strifors, G. C. Gaunnard, B. Brusmark, and S. Abrahamson, IEEE Trans. Ant. Prop. **42**, 453 (1994).
[5] M. Morgan, IEEE Trans. Ant. Prop. **42**, 840 (1994).
[6] W. M. Robertson, G. V. Kopcsay, and G. Arjavalingam, IEEE Microwave Guided Wave Lett. **1**, 379, (1991).
[7] L. Carin, in *Ultra-Wideband, Short-Pulse Electromagnetics*, edited by H. Bertoni (Plenum, New York, 1993), p. 37.
[8] D. Kralj and L. Carin, Appl. Phys. Lett. **62**, 1301 (1993).
[9] A. Rahman, D. Kralj, L. Carin, M. R. Melloch, and J. M. Woodall, Appl. Phys. Lett. **64**, 2178 (1994).
[10] D. Grischkowsky, S. Keiding, M. van Exter, and Ch. Fattinger, J. Opt. Soc. Am. B **7**, 2006 (1990).
[11] P. Uhd Jepsen and S. R. Keiding, Opt. Lett. **20**, 807 (1995).
[12] R. F. Harrington, *Time Harmonic Electromagnetic Fields* (McGraw-Hill, New York, 1961).
[13] L. B. Felsen and N. Marcuvitz, *Radiation and Scattering of Waves* (IEEE, New York, 1973).
[14] D. E. Barrick, in *Radar Cross Section Handbook*, edited by G. T. Ruck (Plenum, New York, 1970).
[15] Aircraft diagrams from *Jane's All the Worlds Aircraft*, with permission from Jane's Information Group Ltd., Sentinel House, U. K.